Electronic Supplementary Material (ESI) for Journal of Materials Chemistry A.

Supplementary Materials for

Thermo-osmotic Ionogel enabled High-efficiency Harvesting of Low-grade Heat

Wei Li,[a] Yuchen Liu,[a] Zimeng Zhang,[a] Ruochen Liu,[b] Jingjing Qiu,[c] Shiren Wang *[a,b]

[a]*Department of Industrial and Systems Engineering, Texas A&M University, College Station, TX 77843, United States.*

[b]*Department of Materials Science and Engineering, Texas A&M University, College Station, TX 77843, United States.*

[c]*Department of Mechanical Engineering, Texas Tech University, Lubbock, TX 79409, United States.*

**Correspondence to: s.wang@tamu.edu*

This PDF file includes:

Supplementary Text
Figs. S1 to S14
Tables S1 to S3

Supplementary Text

1. Comparison of ion flow rate driven by ion gradient (Δc) and temperature gradient (ΔT)

Generally, the movement of ions in a solution is driven by both the concentration gradient (osmotic driven mass diffusion, described by the Fick's Law) and the thermal gradient (thermal driven mass diffusion, defined by the Soret Effect). The mass flux can be written as the following equation [1]:

$$J = -\rho D\frac{\partial c}{\partial x} - \rho D_T c_0(1 - c_0)\frac{\partial T}{\partial x} \quad \text{(S1)}$$

To investigate and compare the mass flux driven by the concentration gradient and the thermal gradient respectively, the Eq. s1 can be divided as:

$$J_C = -\rho D\frac{\partial c}{\partial x} \quad \text{(S2)}$$

$$J_T = -\rho D_T c_0(1 - c_0)\frac{\partial T}{\partial x} \quad \text{(S3)}$$

The Eq. s2 explains the mass diffusion of the Fick's Law where ρ is the density of the solution, c is the mass fraction of the reference component, and D is the molecular diffusion coefficient at the isothermal condition. The Eq. s3 describes the Soret Effect which is proportional to the temperature gradient $\frac{\partial T}{\partial x}$, where D_T is the thermo-diffusion coefficient and c_0 is the fraction of one component.

Here, we numerically investigated the mass flux of two factors respectively for $LiNO_3$-$3H_2O$ solution. The parameter for the calculation was quoted from reference [2].

For Fick's Law term J_C, the mass diffusion coefficient D can be expressed by Stokes-Einstein Equation where the ion of Li^+ and NO_3^- can be regarded as a sphere:

$$D = \frac{k_B T}{6\pi\eta r} \quad \text{(S4)}$$

Where $k_B$is Boltzmann's constant, T is the absolute temperature, η is the dynamic viscosity and r is the radius of the spherical particle. By combining the Eqs. s2 and s4, the mass flux driven by concentration gradient $\frac{\partial c}{\partial x}$ was calculated, as shown by the solid lines in Fig. 1a. The red, orange, purple and pink lines represent the mass flux between $LiNO_3$-$3H_2O$ solution and water (Δc = 0.561) when the separation membrane thickness is 30 um, 100 um, 500 um, and 1000 um, respectively.

For Soret Effect term J_T, the thermo-diffusion coefficient D_T can be estimated by the following equation:

$$D_T = D \cdot S_T \quad \text{(S5)}$$

Where S_T is the Soret coefficient, and its absolute value is about 10^{-3}– 10^{-2} K^{-1}. According to the literature [2], the Soret coefficient of $LiNO_3$ solution was estimated as 0.005. Based on this, the $\frac{\partial T}{\partial x}$

driven mass flux was able to be calculated. The dashed green and blue lines in Fig. 1a indicate the mass flux driven by ΔT of 50K and 20K, respectively. The length of the cell was set as 1 cm.

As shown in Fig. 1a, the mass flux that is driven by the concentration gradient is approximately two orders of magnitude larger than that driven by the temperature gradient. Based on this calculation, we conceived the TOI composite and expected it to harvest low-grade heat efficiently.

2. Theoretical prediction of energy conversion efficiency of TOI system based on laws of thermodynamics

The energy conversion of the TOI system can be divided into two steps, that is, converting thermal energy into chemical potential (salinity gradient energy) and then converting the chemical potential into electric energy. Thus, the energy conversion efficiency of TOI system (η) is the product of the energy conversion efficiency between heat and chemical potential (η_1) and the energy conversion efficiency between chemical potential and electric energy (η_2), expressed as:

$$\eta = \eta_1 \eta_2 \tag{S6}$$

$$\eta_1 = \frac{\Delta_{mix} G}{Q_H} \tag{S7}$$

$$\eta_2 = \frac{W_{out}}{\Delta_{mix} G} \tag{S8}$$

Where Q_H is the energy input to melt the crystalline salt hydrate and build the salinity gradient, and Q_H is proportional to the enthalpy of melting (ΔH). $^{\Delta_{mix}}G$ is the Gibbs free energy change during the mixing, and it represents the chemical potential of the salinity gradient. E_{out} is the output electric energy.

The electrochemical energy conversion efficiency (η_2) corresponding to the maximum power generation can also be calculated as [3]:

$$\eta_2 = \frac{1}{2} S^2 \tag{S9}$$

Where S is the ion selectivity of the ion exchange membrane. In this research, the selectivity of commercial CEM is around 95%, thus η_2 is estimated to be 0.45.

For Eq. S7, $^{\Delta_{mix}}G$ represents the chemical potential of the spontaneous osmotic driven mixing process, which combines two physical effects, the enthalpy of mixing term ($^{\Delta_{mix}}H$) and the entropy of mixing term ($T^{\Delta_{mix}}S$):

$$\Delta_{mix} G = \Delta_{mix} H - T \Delta_{mix} S \tag{S10}$$

Where T is the ambient temperature, $^{\Delta_{mix}}S$ represents the entropy change of random mixing process.

For an ideal solution without chemical reaction, $^{\Delta_{mix}}H$=0, so the Gibbs free energy of mixing is only determined by the entropy term:

$$\Delta_{mix} G = -T \Delta_{mix} S \tag{S11}$$

As for the TOI composite in this study, $^{\Delta_{mix}}S$ is the entropy change of the TOI composite from the initial state to the equilibrium state. In the initial state, the ion concentrations in high-salinity ionogel (HSI) and low-salinity hydrogel (LSH) are 18.4 mol/kg and 0.1 mol/kg, respectively. In the

equilibrium state, the ion concentrations in HSI and LSH are the same, which means the ion cannot spontaneously diffuse from HSI to LSH. $^{\Delta_{mix}}S$ is expressed as:

$$\Delta_{mix}S = (\Delta_{mix}S_{HE} + \Delta_{mix}S_{LE}) - (\Delta_{mix}S_{HI} + \Delta_{mix}S_{LI}) \quad \text{(S12)}$$

Where $^{\Delta_{mix}}S_{HE}$ and $^{\Delta_{mix}}S_{LE}$ are the entropy of mixing of HSI and LSH in equilibrium state, respectively, $^{\Delta_{mix}}S_{HI}$ and $^{\Delta_{mix}}S_{LI}$ are the entropy of mixing of HSI and LSH in the original state, respectively.

The TOI system composite can be regarded as a trinary mixture composed of Li^+, NO_3^- and H_2O. $^{\Delta_{mix}}S_i$ can be calculated according to the following formula [4]:

$$\Delta_{mix}S_i = -n_i R(x_{H_2O} ln(x_{H_2O}) + x_{Li} ln(x_{Li}) + x_{NO_3} ln(x_{NO_3})) \quad \text{(S13)}$$

Where R = 8.314 $Jmol^{-1}K^{-1}$. i represents a specific system under specific condition, such as HSI under initial condition ($^{\Delta_{mix}}S_{HI}$). ^{n_i} is the molar mass of Li^+, NO_3^- or H_2O at condition i. ^{x_i} is the molar mass ratio of Li^+, NO_3^- or H_2O.

In a typical TOI system configuration (Table S1), $^{\Delta_{mix}}S$ is 0.118 JK^{-1} (Eqs. S12 and S13, Table S2). Based on Eqs. S6 to S11, at a certain temperature and TOI system configuration, the theoretical thermo-electric conversion efficiency (η) of TOI system is only negatively related to the melting of enthalpy of $LiNO_3$-$3H_2O$. For instance, when pure $LiNO_3$-$3H_2O$ is used as the crystalline salt hydrate, ΔH is 32.5 kJ/mol. At 90 °C, η_1 and η are theoretically estimated to be 19.3% and 8.7%, respectively.

When PAM is incorporated into $LiNO_3$-$3H_2O$, the resulting ionogel has a lower enthalpy of melting (Fig. 2a), which will improve the overall thermo-electric conversion efficiency. For instance, as the polymer concentration increases to 10 wt%, the enthalpy of melting decreases to 20.8 kJ/mol due to the increased interaction between PAM and salt hydrate. At 90 °C, η_1 and η are theoretically estimated to be 30.2% and 13.6%, respectively.

3. Peak energy conversion efficiency of TOI cell based on maximum output power

Assuming a constant ion gradient, the heat-to-electric energy conversion efficiency of TOI cell (η_E) can be calculated by the ratio of output electric power to input thermal power:

$$\eta_E = \frac{P_{out}}{P_{input}} \quad \text{(S14)}$$

P_{out} is the output power of the TOI cell. When the output voltage is chosen as half of the open-circuit voltage ($V_{out} = 0.5V_{oc}$), P_{out} can reach the maximum value, expressed as:

$$P_{out} = \frac{{V_{out}}^2}{R} = \frac{\sigma_e A {V_{OC}}^2}{4\Delta x} \quad \text{(S15)}$$

Where σ_e is the ionic conductivity of the TOI composite, A is a cross-sectional area of the CEM, and Δx is the distance between the electrodes.

The input thermal power (P_{input}) corresponding to the P_{out} consists of two parts, namely the heat absorbed for ionic crystal transition (P_{melt}) in the phase transition and the thermal diffusion (P_{diff}) in the electric power generation, which can be determined by the following formula:

$$P_{input} = P_{melt} + P_{diff} \quad \text{(S16)}$$

Where P_{melt} is the energy consumption during the melting of salt hydrate corresponding to the electric power generation stage, which can be calculated by the following formula:

$$P_{melt} = \Delta H D_c = \frac{\Delta H I}{F} \quad \text{(S17)}$$

Where ΔH is the enthalpy of melting, D_c is the cation diffusivity in mol/s, which represents the molar mass of cation diffused from the ionogel to the hydrogel per unit time. D_c can be calculated by dividing the current I by Faraday constant F =96485 Cmol^{-1}.

P_{diff} is the heat transfer of the TOI cell caused by thermal diffusion in electric power generation stage, which can be calculated by Fourie's law:

$$P_{diff} = \kappa A \frac{\Delta T}{\Delta x} \quad \text{(S18)}$$

Where κ is the thermal conductivity of the TOI composite.

Therefore, the energy conversion efficiency can be expressed as [5]:

$$\eta_E = \frac{\frac{\sigma_e A {V_{OC}}^2}{4\Delta x}}{\frac{\Delta H I}{F} + \kappa A \frac{\Delta T}{\Delta x}} = \frac{\sigma_e {V_{OC}}^2}{4(\frac{\Delta H I \Delta x}{FA} + \kappa \Delta T)} \quad \text{(S19)}$$

In a typical TOI cell, ΔH = 20800 J/mol, Δx =0.008 m, and A=0.014 m*0.014 m=0.000196 m^2. When TOI cell worked at 90 ^{o}C, σ_e= 19.46 S/m, V_{OC}=0.524 V, ΔT =20.04 ^{o}C, I_{SC} = 0.00009A, κ=0.588 Wm^{-1}K^{-1}, resulting in an energy conversion efficiency of 11.17%.

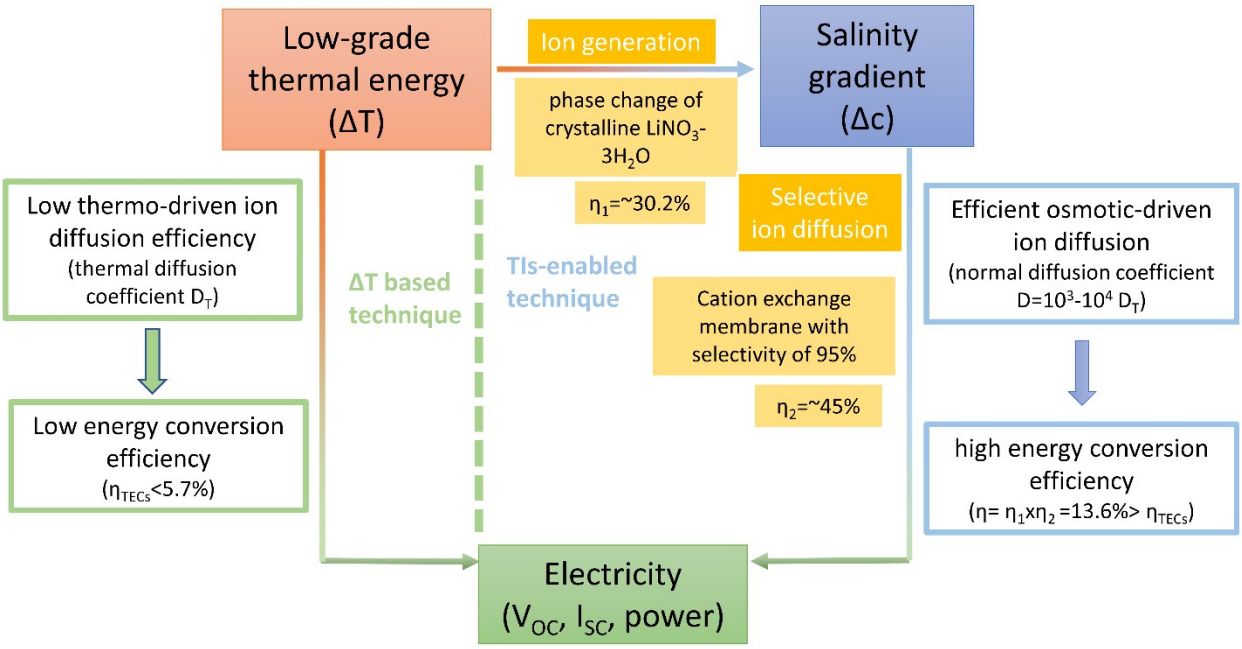

Fig. S1.

Concept and hypothesis of TOI cell for low-grade heat harvesting.

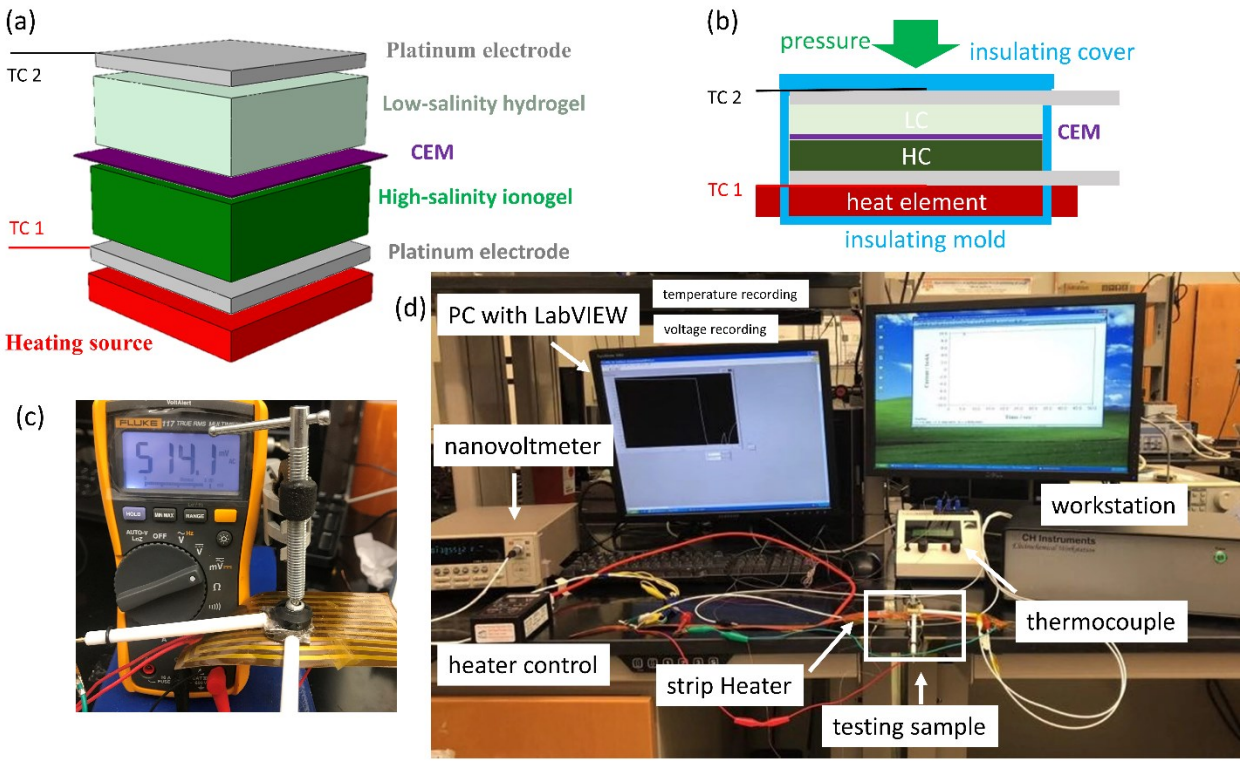

Fig. S2.

TOI cell and thermo-electric energy conversion characterization setup. (a, b) Schematic and (c) photo of TOI cell. (d) Photograph of thermo-electric energy conversion characterization setup. Please note that the TOI composite was encapsulated in a heating-insulating silicone mold in the actual characterization. In fig. S2c, we removed the mold to clearly show the internal structure of TOI composite.

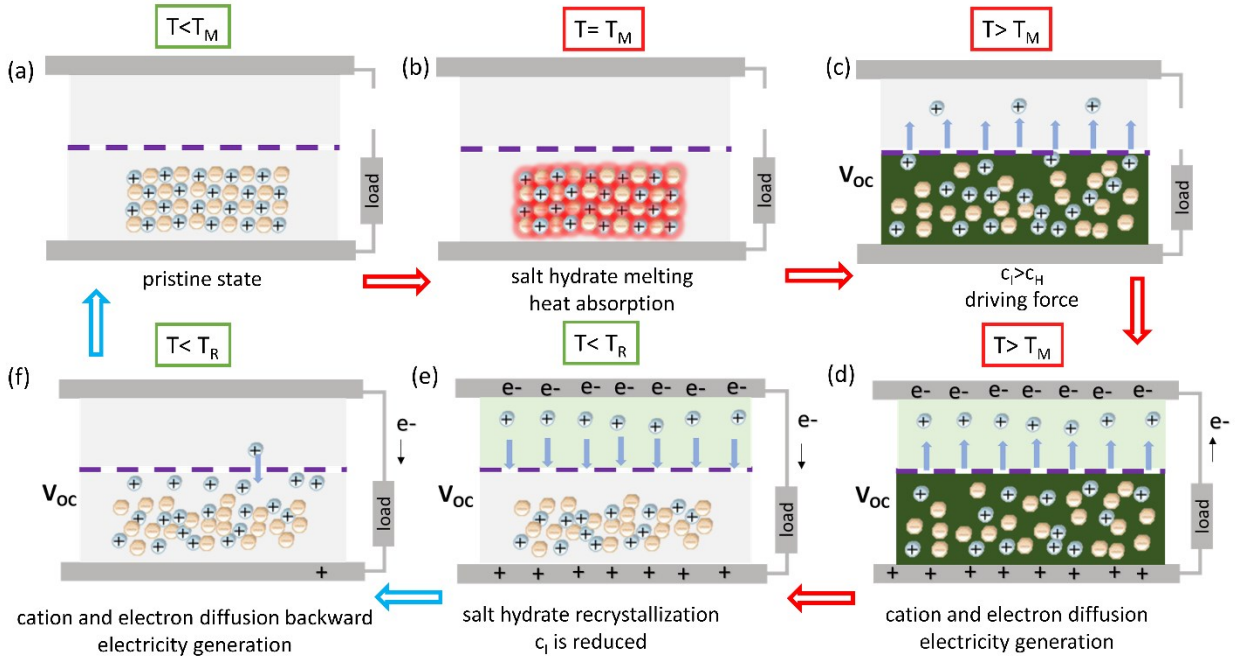

Fig. S3.

Working mechanism of TOI cell. (a) Schematic of TOI cell at initial state, which is composed of crystalline $LiNO_3$-$3H_2O$ ionogel, CEM, 0.1M $LiNO_3$ hydrogel, and symmetric Pt electrodes. (b) Upon heating, the crystalline $LiNO_3$-$3H_2O$ melts and generates $LiNO_3$ solution with a molarity of 18.4 mol/kg, converting the thermal energy into chemical energy in the form of osmotic potential (Δc). (c) With ion gradient as the driving force, CEM selectively allows cations to diffuse from ionogel to hydrogel, thereby generating a voltage. (d) When the electrodes are electrically connected through an external circuit, electrons can transport directionally in the circuit, thereby converting the chemical potential energy into electrical energy. (e, f) As the system temperature decreases below the recrystallization temperature (T_R) of the $LiNO_3$-$3H_2O$, the ionogel will recrystallize and the lithium-ion concentration of the ionogel will decrease and be lower than that of the hydrogel. The reverse ion gradient will push the lithium ions diffuse back into the ionogel and form crystalline $LiNO_3$-$3H_2O$. Afterward, the TOI cell may be restored to its original state and be used to recover low-grade heat again.

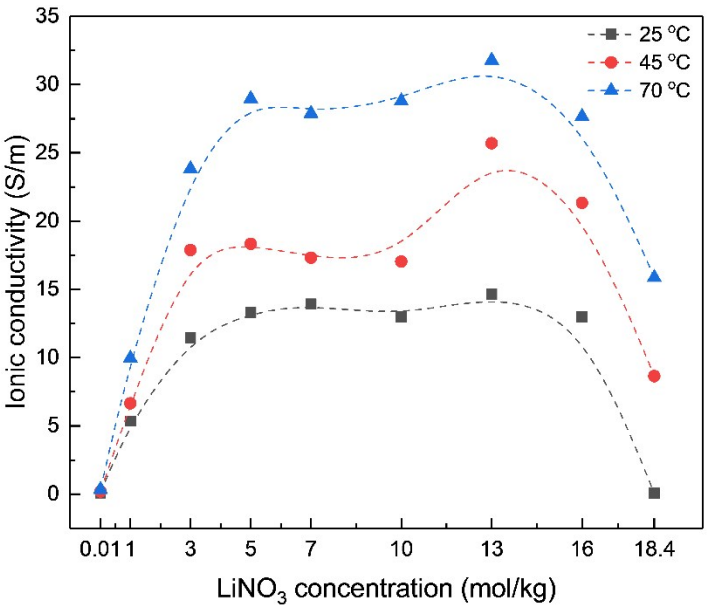

Fig. S4.

Ionic conductivity of $LiNO_3$ solution as a function of salt concentration and temperature. As the salt concentration increased, the ionic conductivity of the $LiNO_3$ solution first increased and then decreased, and reached the maximum value when the salt concentration was 13 mol/kg (fig. S4). The results are well consistent with the reported values in literature [6]. In addition to the salt concentration, increasing the temperature also significantly increased the ionic conductivity. The ionoic conductivity of 1 mol/kg $LiNO_3$ solution is 6.64 S/m at 45 °C. If we assume the ionic activity coefficient (γ) of 1 mol/kg $LiNO_3$ solution is 1, the theoretical ionic conductivity of $LiNO_3$-$3H_2O$ solution (18.4 mol/kg) should be 122 S/m, which is much larger than the measured value of 8.64 S/m, indicating severe ion-pairing formation.

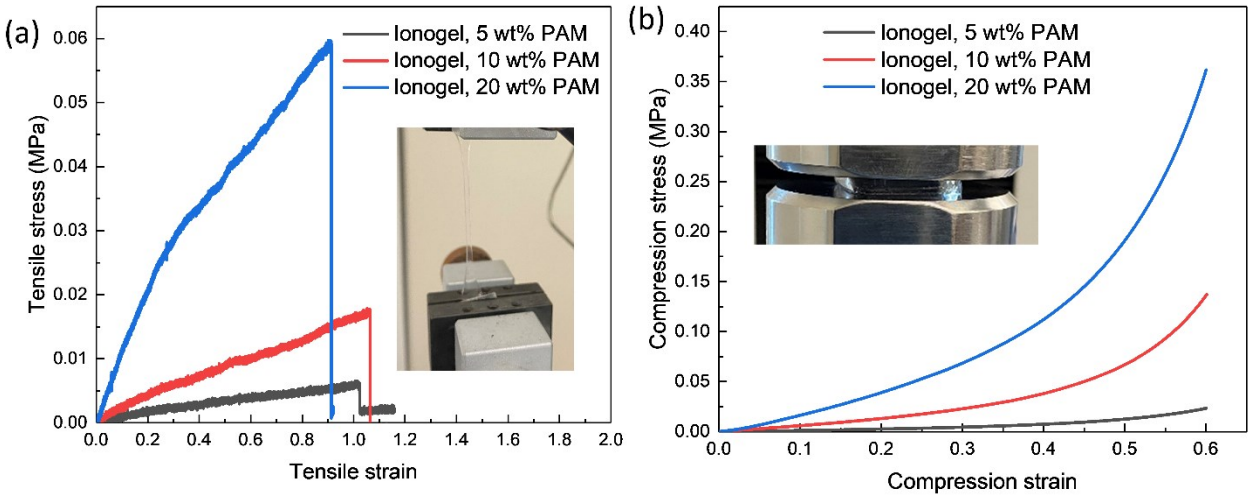

Fig. S5.

Mechanical characterization of ionogel. (a) Tensile stress-strain curve. (b) Compressive stress-strain curve with a maximum compressive strain of 0.6.

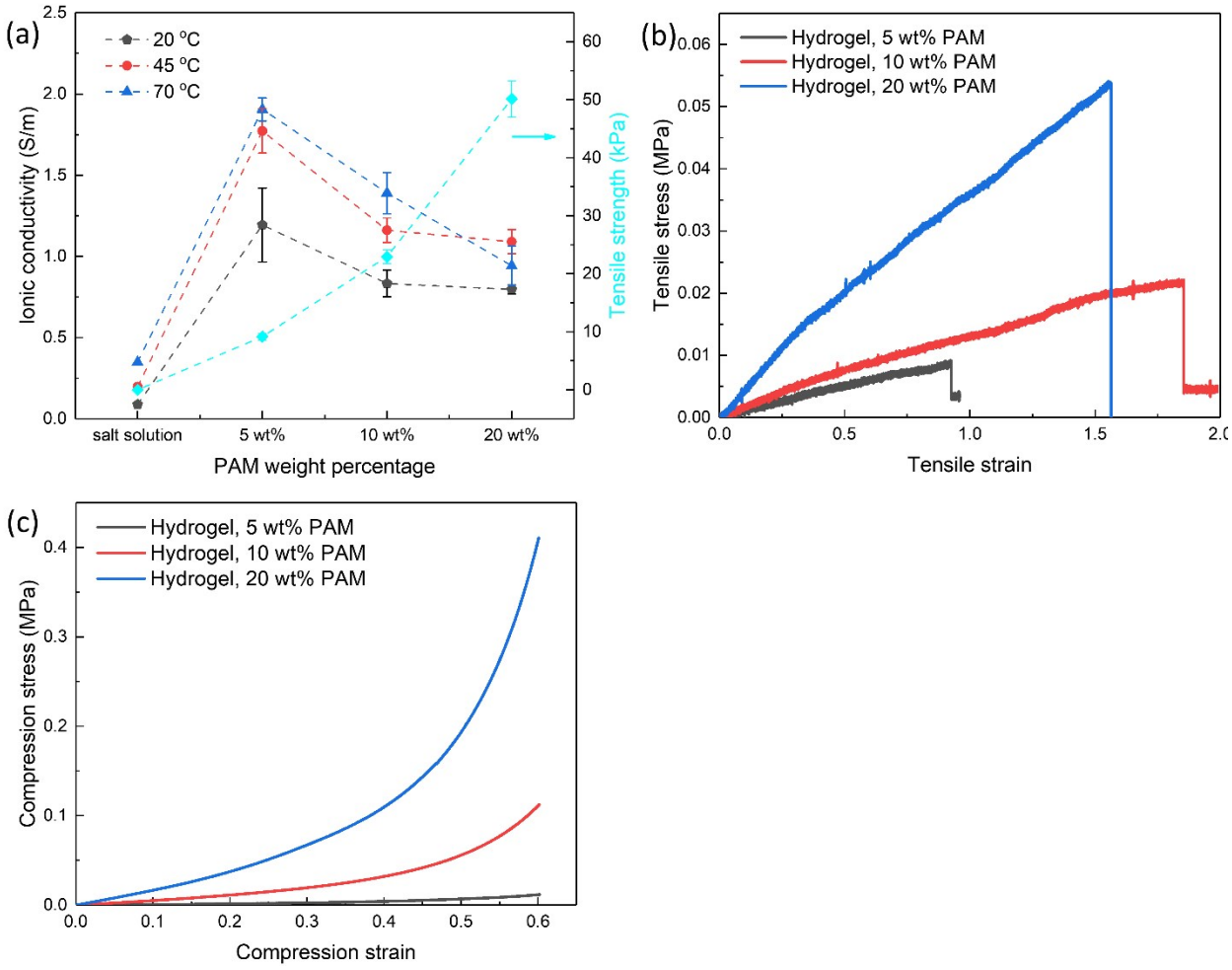

Fig. S6.

Ionic conductivity and mechanical properties of low-salinity hydrogel with various PAM concentration. (a) Ionic conductivity and tensile strength of low-salinity hydrogel (0.1 mol/kg) as a function of PAM concentration. Considering the trade-off between the overall ionic conductivity, salinity gradient, and mechanical properties of TOI composite, 10 wt% PAM with 0.1 mol/kg $LiNO_3$ was selected for low-salinity hydrogel. (b) Tensile stress-strain curve. (c) Compressive stress-strain curve with a maximum compressive strain of 0.6.

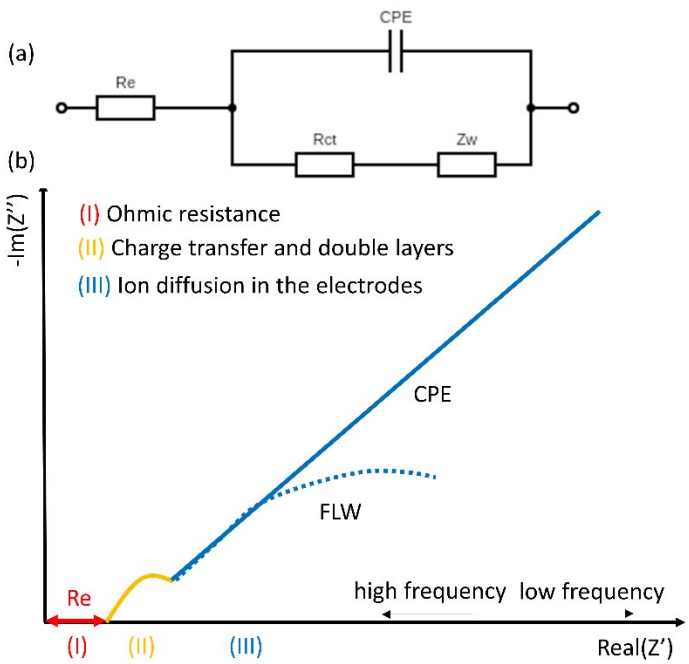

Fig. S7.

Impedance spectrum and Warburg model. (a) Schematic of equivalent Randle circuit. Re is the ohmic resistance of TOI cell, Rct is resistance due to charge transfer, CPE is a constant phase element due to capacitance of double layer, Zw is Warburg impedance (mass-transfer). (b) Typical impedance spectrum to model the impedance behavior.

From high to low frequency, the impedance of electrode/electrolyte/electrode structure is mainly caused by ohmic resistance (I), double layer and charge transfer effects at the interfaces (II) and ion diffusion within the electrodes (III). Specific, the low frequency diffusion behavior is typically modelled by a finite length Warburg (FLW) and a constant phase element (CPE). At low frequency region, Pt/ionogel/CEM/hydrogel/Pt showed a smaller finite length Warburg, indicating there existed a spontaneous ion diffusion from the ionogel to hydrogel due to the ionic gradient [7].

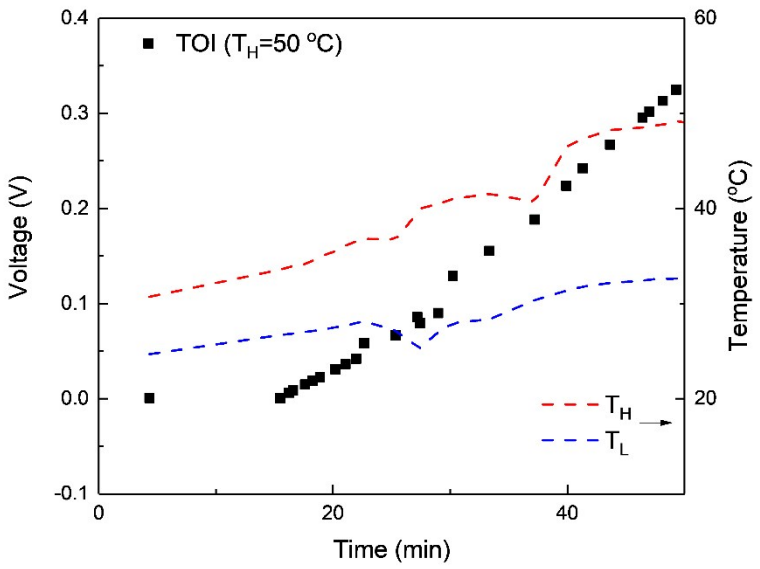

Fig. S8.

Real-time V_{OC} recording of TOI cell with a 50 °C heat source. T_H and T_L represent the temperature of the hot and cold side of the TOI cell, respectively.

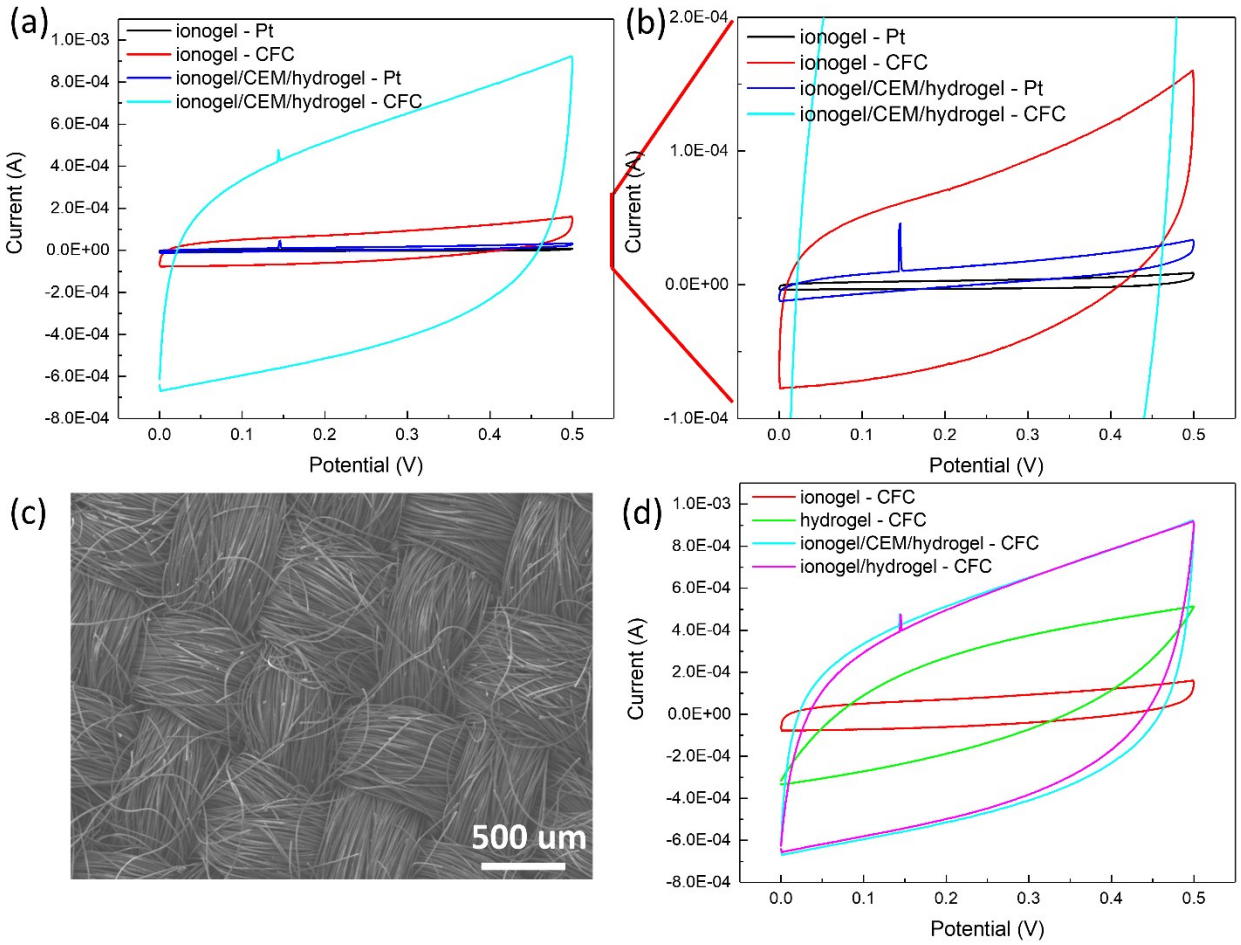

Fig. S9.

Cyclic voltammetry of the TOI composite with Pt and carbon fiber cloth (CFC) electrodes. (a, b) Cyclic voltammetry of $LiNO_3$-$3H_2O$ ionogel and ionogel/CEM/hydrogel composite. (c) Morphology of carbon fiber cloth (JEOL JSM-7500F). (d) Cyclic voltammetry of 0.1M $LiNO_3$ hydrogel, $LiNO_3$-$3H_2O$ ionogel, ionogel/hydrogel and ionogel/CEM/hydrogel with CFC as electrodes. The heat source is at 35 ^oC, which ensure the $LiNO_3$-$3H_2O$ is in melting status.

As the cyclic voltammetry shown in figs. S9a and S9b, the current of the CFC/ionogel/CEM/hydrogel/CFC structure was one order larger than that of the Pt/ionogel/CEM/hydrogel/Pt in the I-V curve. It was because the porous CFC electrode (fig. S9c) could store more ions than the smooth Pt electrode. No matter the electrode was Pt or CFC, the I-V curve of ionogel/CEM/hydrogel was approximately rectangular, indicating that the charging and discharging of TOI composite were non-Faraday processes [8]. In addition, the I-V curve of single ionogel and single hydrogel didn't appear redox peak (fig. S9d) but showed a typical surface-controlled non-Faraday process [9], which also proved that there was no redox reaction on the hydrogel/electrode or ionogel/electrode interface in the TOI composite.

It should be noted that there was a sharp "peak" near 0.15V during the charging process, but no peak appeared during the discharging process. This peak was caused by the Δc between ionogel and hydrogel. At the beginning of the charging process, the cations on the ionogel/hydrogel

interface tend to migrate from ionogel to hydrogel since the electromotive force was smaller than the osmotic pressure. When the charging voltage increased to around 0.15 V, the electromotive force was larger than the osmotic pressure, so the cations on the ionogel/hydrogel interface migrated from the hydrogel back to the ionogel. This change in direction of cation movement resulted in a sudden increase in current, thereby showing a “peak” on the I-V curve.

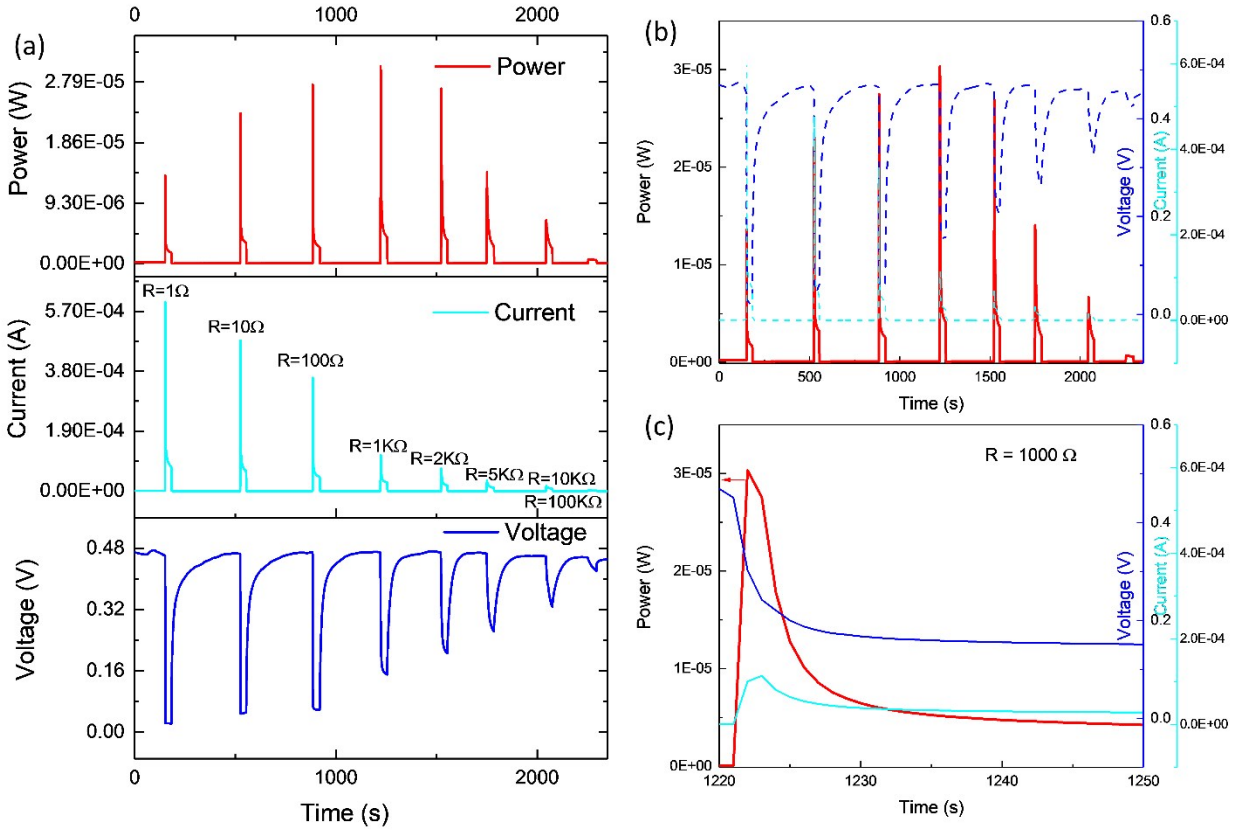

Fig. S10.

Voltage, current and power of TOI cell during discharge process. (a, b) Voltage, current and power of TOI cell with different external resistors. (c) Voltage, current and power of TOI cell as the external resistor was 1000 Ω. The heat source was at 90 °C, and the electrode was CFC. When the TOI cell was at the open-circuit status, the current and output power was 0, and the voltage recovered. Once the TOI cell was connected to various external loads, there was current during the discharging process. It should be noted that the ammeter and voltmeter kept recording during the cyclic open circuit-discharging process.

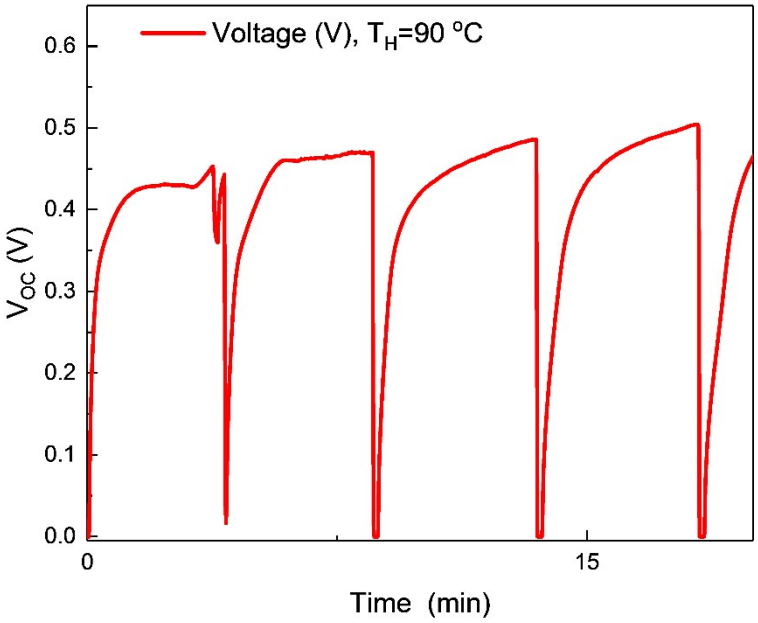

Fig. S11.

Voltage of TOI cell during open-circuit and short-circuit cycling. The heat source was at 90 °C.

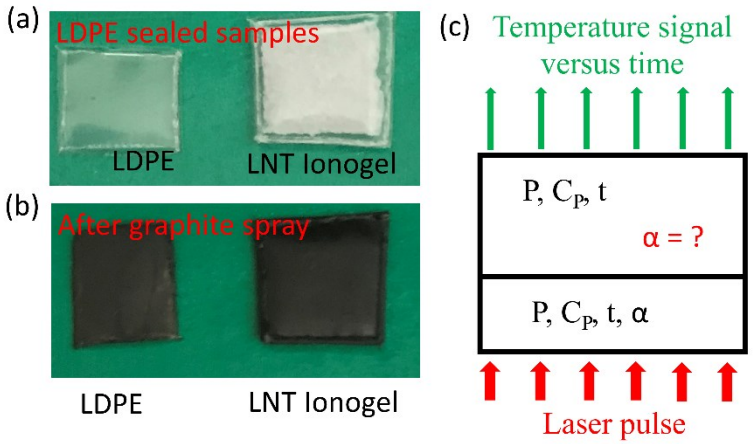

Fig. S12.

Thermal conductivity measurement setup. (a) Ionogel was sealed by a low-density polyethylene (LDPE) film to prevent water evaporation during measurement. (b) A very thin graphite coating was applied on both sides of the sample to act as an absorber on the front and an emitter on the back. (c) Schematic diagram of the double-layer mode applied to measure the unknown thermal diffusivity of the ionogel.

Laser flash is a widely used transient method to determine the thermal diffusivity of solid and liquid materials [10]. During the measurements, the instantaneous light was used as a heat source to raise the temperature of the front side of the sample while an infrared detector is applied to record the temperature response on the rear side. A very thin graphite coating was applied on both faces of the samples to act as an absorber on the front side and an emitter on the rear side. Considering the ionogel would lose heat via water evaporation during the measurement, a low-density polyethylene (LDPE) film was employed to seal the ionogel (fig. S12). By defining the thermal behaviors of LDPE in advance, a double layer model was applied to measure the unknown thermal diffusivity of the ionogel.

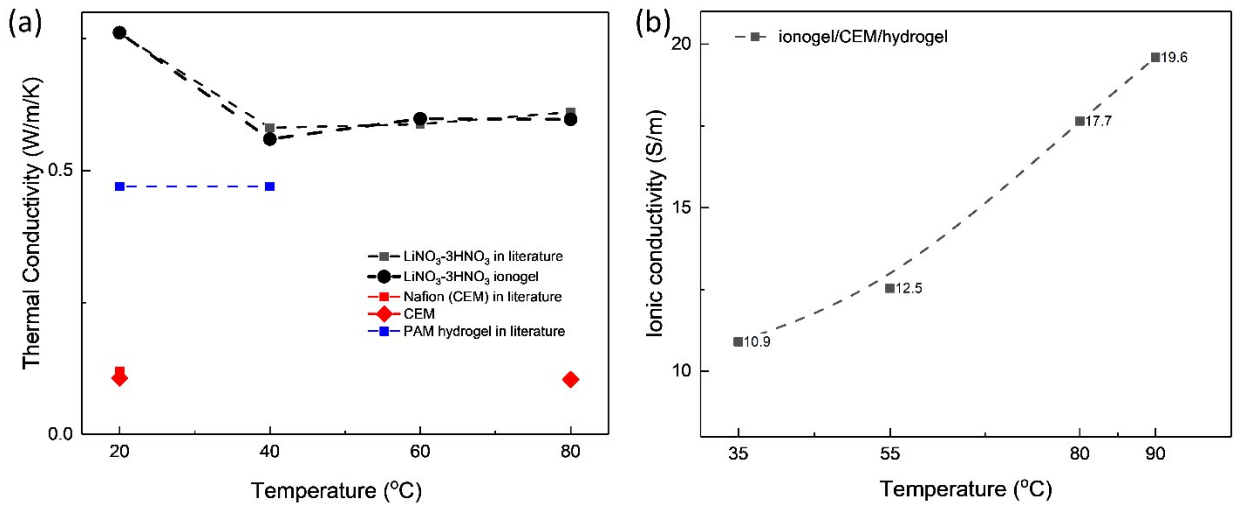

Fig. S13.

Thermal conductivity and ionic conductivity of TOI composite. (a) The thermal conductivities of ionogel, hydrogel, and CEM, which are consistent with the reported thermal conductivity values of $LiNO_3$-$3H_2O$ [2], PAM hydrogel [11] and CEM [12] in literature. In the efficiency calculation, the thermal conductivity of TOI composite was set at 5.88 $Wm^{-1}K^{-1}$. (b) The effective ionic conductivity of TOI composite as a function of hot-end temperature.

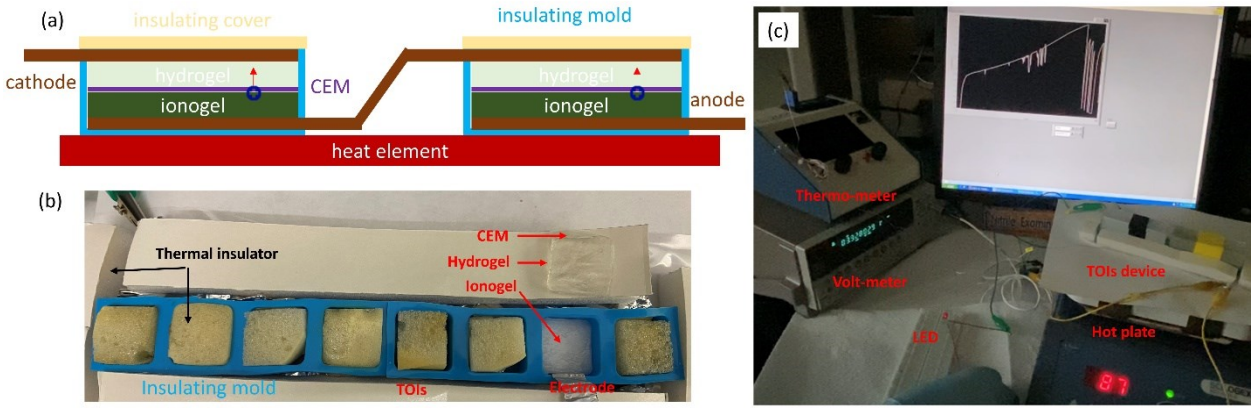

Fig. S14.

Fabrication and characterization setup of TOI device, which are composed of 8-units TOI composites connected in series. (a, b) Schematic and experimental photo of the multi-unit TOI composites. (c) The TOI device was thermally charged on a hot plate at 90 ^{o}C, which generated a voltage of 3.9 V and successfully powered a LED.

Table S1.

Structure parameters of a typical TOI cell configuration.

Item	cross-section	thickness	density	n ($LiNO_3$)	n (H_20)
unit	cm*cm	cm	g/cm^3	mol	mol
Ionogel with $LiNO_3$-$3H_2O$	1.4*1.4	0.3	1.425	0.0068	0.020
Hydrogel with 0.1M $LiNO_3$	1.4*1.4	0.5	1	6.17E-05	0.054

Table S2.

Changes in the mixing entropy of hydrogel and ionogel during salinity equilibrium.

Item	x (Li^+)	x (NO_3^-)	x (H_2O)	n (total)	Δmix S (J)
HSI-initial	0.2	0.2	0.6	0.03406	0.2691
LSH-initial	0.00113	0.00113	0.9977	0.05457	0.0079
HSI-equilibrium	0.1	0.1	0.8	0.02555	0.1357
LSH- equilibrium	0.06847	0.06847	0.8631	0.06308	0.2592

Table S3.

Electrical characterization of TOI cells.

Sample	Voltage (V)	T_H (°C)	T_L (°C)	ΔT (°C)	V/ΔT (mV/K)	Schematic of set-up
HC-CEM-LC solution	0.099±0.002	Isothermal at 35 °C		NA	NA	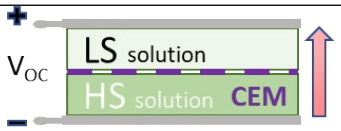
HSI-CEM-LSH	0.213±0.012	Isothermal at 35 °C		NA	NA	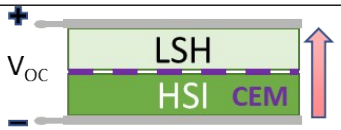
HSI	0.166±0.005	74.06	58.31	15.75	10.53±0.23	
LSI	0.077±0.004	65.65	51.52	14.13	5.46±0.29	
HSI-CEM-LSH	0.267±0.013	46.8	32.9	13.9	19.21±1.24	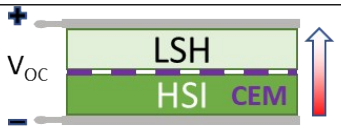
HSI-CEM-LSH	0.428±0.015	74.06	57.12	16.94	25.28±0.83	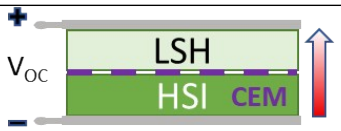
HSI-CEM-LSH	0.497±0.011	86.9	67.5	19.4	25.61±0.55	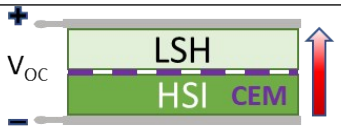

References

1. J. K. Platten, 2006.
2. P. J. Shamberger and T. Reid, *Journal of Chemical & Engineering Data*, 2012, **57**, 1404-1411.
3. D.-K. Kim, C. Duan, Y.-F. Chen and A. Majumdar, *Microfluidics and Nanofluidics*, 2010, **9**, 1215-1224.
4. I. Prigogine, *New York: Interscience*, 1967.
5. H. Zhou and P. Liu, *ACS Applied Energy Materials*, 2018, **1**, 1424-1428.
6. A. Campbell, G. Debus and E. Kartzmark, *Canadian Journal of Chemistry*, 1955, **33**, 1508-1514.
7. M. Oldenburger, B. Beduerftig, A. Gruhle, F. Grimsmann, E. Richter, R. Findeisen and A. Hintennach, *Journal of Energy Storage*, 2019, **21**, 272-280.
8. T. S. Mathis, N. Kurra, X. Wang, D. Pinto, P. Simon and Y. Gogotsi, *Advanced Energy Materials*, 2019, **9**, 1902007.
9. N. Elgrishi, K. J. Rountree, B. D. McCarthy, E. S. Rountree, T. T. Eisenhart and J. L. Dempsey, *Journal of chemical education*, 2018, **95**, 197-206.
10. W. Parker, R. Jenkins, C. Butler and G. Abbott, *Journal of applied physics*, 1961, **32**, 1679-1684.
11. N. Tang, Z. Peng, R. Guo, M. An, X. Chen, X. Li, N. Yang and J. Zang, *Polymers*, 2017, **9**, 688.
12. O. U. Rehman and A. F. Zafar, *Journal of Electrochemical Science and Engineering*, 2017, **7**, 223-235.